AIAA JOURNAL
Vol. 49, No. 8, August 2011

Closed-Loop Control of Lift for Longitudinal Gust Suppression at Low Reynolds Numbers

Wesley Kerstens*
Illinois Institute of Technology, Chicago, Illinois 60616
Jens Pfeiffer†
Technical University of Berlin, 10623 Berlin, Germany
David Williams‡
Illinois Institute of Technology, Chicago, Illinois 60616
Rudibert King§
Technical University of Berlin, 10623 Berlin, Germany
and
Tim Colonius¶
California Institute of Technology, Pasadena, California 91125

DOI: 10.2514/1.J050954

Experiments are conducted to investigate the ability of variable-pressure pulsed-blowing actuation to maintain a constant lift force on a low-aspect-ratio semicircular wing in a longitudinally gusting flow. Dynamic models of the lift response to actuation and the lift response to longitudinal gusting are obtained through modern system identification methods. Robust closed-loop controllers are synthesized using a mixed-sensitivity loop-shaping approach. An additional feedforward disturbance compensator is designed based on a model of the unsteady aerodynamics. The controllers show suppression of lift fluctuations at low gust frequencies, $f < 0.8$ Hz (reduced frequency, $k < 0.09$). At higher frequencies, the control performance degrades due to limitations related to the time for a disturbance, created by the actuators, to convect over the wing and establish the flowfield that leads to enhanced lift on the wing.

Nomenclature

c	=	chord length, m
C_L	=	lift coefficient; $L(qS)^{-1}$
C_{pj}	=	actuator supply pressure coefficient; $p_j q^{-1}$
f	=	frequency, Hz
f^+	=	dimensionless frequency; fc/U
j	=	imaginary variable; $(-1)^{1/2}$
K	=	transfer function gain parameter
k	=	reduced frequency; $\pi fc/U$
L	=	lift force, perpendicular to flow direction, N
p_j	=	actuator supply pressure, kPa
q	=	dynamic pressure; $\frac{1}{2}\rho U^2$
r	=	reference lift, N
S	=	wing planform area, m^2
s	=	Laplace variable
T	=	transfer function time constant parameter
t^+	=	dimensionless time; tU/c
U	=	flow speed, m/s
u_j	=	actuator jet velocity, m/s
y_d	=	lift due to unsteady aerodynamics, N
y_p	=	lift output from plant, N
α	=	wing angle of attack, °
Δt^+	=	dimensionless actuator pulse duration
θ	=	time delay, s
ω	=	circular frequency, rad/s; $2\pi f$

Presented as Paper 2010-4969 at the 5th Flow Control Conference, Chicago, IL, 28 June–1 July 2010; received 23 September 2010; revision received 14 January 2011; accepted for publication 5 March 2011.

*Graduate Research Assistant, Mechanical and Aerospace Engineering Department. Student Member AIAA.
†Graduate Research Assistant, Chair of Measurement and Control. Student Member AIAA.
‡Professor, Mechanical and Aerospace Engineering Department. Associate Fellow AIAA.
§Professor, Chair of Measurement and Control. Member AIAA.
¶Professor, Mechanical Engineering Department. Associate Fellow AIAA.

I. Introduction

ACTIVE flow control (AFC) of lift in unsteady flow situations offers a number of performance benefits that are not achievable with a quasi-steady approach, such as extending the range and endurance of flight vehicles by energy extraction from atmospheric disturbances, suppressing the unsteady lift fluctuations caused by gusting flows, enhancing maneuverability, and enabling pinpoint perch landings. The focus here is on suppressing lift fluctuations in an unsteady freestream (simulating longitudinal gusts). In addition to providing a demonstration of the benefits and limitations of AFC in unsteady flows, gust-suppression techniques have the practical benefit of reducing loads on aircraft and enabling more stable platforms for sensors.

Gust loads are produced by instantaneous changes in angle of attack or airspeed caused by atmospheric turbulence. In the industry, statistical approaches [1] are used to estimate the size of the loads acting on the flight vehicle based on an assumed form for the turbulence spectrum. However, the time averaging involved in obtaining the load statistics does not allow this approach to be useful as a gust-suppression controller. A controller capable of detecting an instantaneous gust and responding in a way that counteracts the deviation from the turbulence requires a sensor to detect the gust, an actuator to modify the flow around the flight vehicle, and a control algorithm to coordinate the sensor(s) and actuator(s).

The ability of AFC techniques to delay separation or force reattachment of a separated flow over a surface is well established for steady-state conditions [2,3]. However, when the flow becomes unsteady during maneuvering, or in gusting flow conditions, then quasi-steady approximations quickly break down. Deviations from quasi-steady performance appear in the lift as time delays and differences in amplitudes relative to the quasi-steady predictions.

These deviations must be modeled for successful control. In a previous investigation [4], we identified three requirements for improving lift control in unsteady flows: 1) an improved model for the flow response to actuation (plant); 2) a model of the unsteady aerodynamic effects; and 3) controllers that compensate for those effects. In this paper, each of these elements is investigated relative to suppressing lift fluctuations in a longitudinally gusting freestream.

Models for the flow response to actuation can be obtained from the transient output signals following step or pulse inputs from an actuator. There have been several investigations into the transient response of two-dimensional separated flows. Darabi and Wygnanski [5,6] studied the reattachment and detachment processes on a generic two-dimensional flap by using step inputs from a voicecoil-type actuator. Transient reattachment and separation processes were found to last substantially longer than the duration of actuation. They found that many features of the transient dynamics could be scaled by the lift coefficient C_l and convective time $t^+ = tU/c$. At the onset of actuation, an initial lift reversal preceding the rapid lift increase was seen, and a lift overshoot connected with the termination of actuation that had similarities with a dynamic stall vortex. Amitay and Glezer [7] studied the effects on circulation of very-short-duration pulses ($\Delta t^+ < 0.1$) from a synthetic jet actuator on separated flow over a two-dimensional symmetric airfoil. Measurements of the circulation showed that the separated flow was receptive to short-duration pulses much shorter than the timescale of the wake oscillation frequency. Detailed particle image velocimetry measurements of the vorticity field associated with the transient reversals in circulation at the onset of actuation were obtained by Brzozowski and Glezer [8]. Woo et al. [9] used a sequence of short pulses to achieve larger increases in circulation by capitalizing on the long-duration relaxation process. Transient effects on low-aspect-ratio finite-span wings were investigated by Williams et al. [10]. Those studies showed that increases in the lift coefficient on three-dimensional wings were comparable to two-dimensional airfoils, and the transient dynamics of wings showed similar lift reversals and long relaxation times, as seen in the two-dimensional flows.

The lift response to short-duration pulses of actuation approximates the impulse response, and this can be used as a kernel in a convolution to predict the lift response to more complex input signals [10,11]. More modern system identification techniques [12] were used by Williams et al. [4] and Kerstens et al. [13] in order to obtain more practical black-box models of the separated flow dynamics. These investigations showed that the linear approach could be quite useful in predicting the lift response over a wide range of forcing conditions, provided the angle of attack was fixed. A similar approach is used in this work and is described in Sec. III.A.

The second requirement for improving control in unsteady flows is a model for unsteady aerodynamic effects. The classical approach for predicting the response to longitudinal flow unsteadiness was derived by Greenberg [14] in an extension to Theodorsen's [15] theory. The theory assumes the flow is two-dimensional and attached, and the wake is planar. These assumptions are violated when dealing with the separated flow over low-aspect-ratio wings. Consequently, it is necessary to use experimental measurements to obtain practical models for the unsteady aerodynamic effects. Leishman [16] and van der Wall [17] provided extensive descriptions of the limitations and values of the various unsteady aerodynamic theories.

Different approaches for dealing with the unsteady aerodynamics were attempted in our earlier studies, with varying results. A quasi-steady aerodynamic approach was used by Williams et al. [18] to model the plant dynamics. The bandwidth was limited to reduced frequencies of $k < 0.03$, because unsteady aerodynamics were not modeled. To achieve a higher bandwidth, Williams et al. [19] accounted for the unsteady aerodynamics in an ad hoc manner by experimentally measuring the phase between the velocity and the lift fluctuations at a single reduced frequency, $k = 0.13$. This method showed substantial suppression (17 dB) of a sinusoidally oscillating freestream at $k = 0.13$, although as it was tuned to a single frequency, it was unable to respond to arbitrary velocity variations, i.e., real gusting conditions. Subsequently, a model for the dynamics of the separated flow response to actuation was obtained, but the unsteady aerodynamic effects were left unmodeled. The controller was able to compensate for arbitrary disturbances within a certain bandwidth, but the frequency limit for which this controller was effective was close to quasi-steady conditions due to unmodeled unsteady aerodynamics [4].

The current work further develops closed-loop control to suppress lift fluctuations about a mean flow speed, treated as a cruise flight condition, by using the lift force as the control objective and the actuator pressure as the input. The objectives are to increase the bandwidth of effective control by incorporating an unsteady aerodynamic model and feedforward disturbance compensation, and to demonstrate the suppression of lift fluctuations in a randomly varying velocity field. The experimental setup is described in Sec. II. The modeling of the dynamic response to actuation and the unsteady aerodynamics are described in Sec. III, along with the controller synthesis methods and the results of the closed-loop control experiments. Section IV discusses the results and the limitations imposed by the dynamic response, and the conclusions are presented in Sec. V.

II. Experimental Setup

The experiments were conducted in the Andrew Fejer Unsteady Flow Wind Tunnel at the Illinois Institute of Technology. The wind tunnel is a closed-return type powered by a 40 hp motor with a vector drive controller. Figure 1 shows a schematic of the wind-tunnel test section with the sting-mounted model. The test section dimensions are 0.61 by 0.61 m, with a length of 3.1 m. Flow speeds used during the experiments ranged from 4 to 9 m/s. The highest level of freestream turbulence level was measured to be 0.6% at an average speed of 3 m/s over a bandwidth from 0.1 to 30 Hz. A computer-controlled cascade of shutters located at the downstream end of the test section is used to control the freestream speed oscillations. Oscillation amplitudes up to 10% of the mean speed and frequencies up to 3 Hz are achievable. Steady flow velocities are measured with a pitot-static tube, and dynamic velocities are measured with a hot-wire anemometer. Both sensors are located approximately 1 m upstream of the wing. The forces and moments acting on the wing are measured with a six-component balance (ATI: Nano 17). The uncertainty in the force measurement is based on the repeatability of calibration data and is estimated to be less than 0.01 N.

The wing has a semicircular planform area with a centerline chord of 0.203 m. This planform, in combination with pulsed-blowing actuators, produces a large lift increment above the uncontrolled case, and the lift increment can be varied in a continuous manner by changing the supply pressure to the actuators. The wing was constructed from Duraform® nylon using a 3D Systems selective laser sintering, rapid prototyping machine. The wing is fixed at an angle of attack $\alpha = 20^\circ$ for all of the measurements in this study, which corresponds to a fully separated state. This angle is chosen for the study because it allows for the maximum range of lift control. The baseline flow (without actuation) separates at the leading edge, and the separation region closes well downstream of the trailing edge of the wing. The flow-control actuator is a pulsed-blowing type consisting of 16 Lee microvalves designed to fit into the leading edge of the wing and are operated simultaneously. A Fairchild pressure

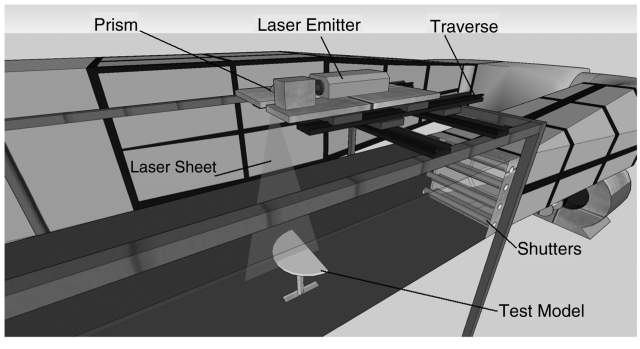

Fig. 1 Schematic of the Andrew Fejer Unsteady Wind Tunnel.

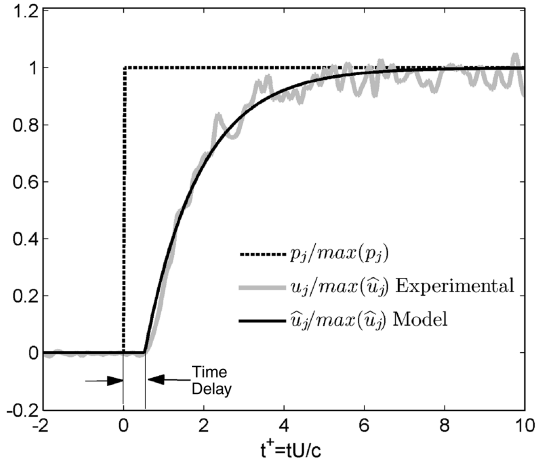

Fig. 2 Jet velocity response $\hat{u}_j$ of identified actuator model compared with measured jet velocity response u_j to a step increase in desired jet pressure p_j plotted against convective time at 7 m/s.

regulator (model TA-6000-004U) regulates the pressure supply to the plenum within the wing. The pressure at the regulator output is measured with an Omega Engineering® (model px139) pressure transducer. The microvalves are operated at 29 Hz, which corresponds to $f+ = 1.0$ at $U = 7$ m/s. The frequency of 29 Hz was initially chosen to avoid exciting a resonant frequency in a previous experimental setup [10]. Further investigation showed that the lift response remained nearly constant once the actuation was sufficiently fast. Steady blowing reduces the lift force below the unactuated baseline value. The pressure within the plenum is varied to change the actuation amplitude. Varying the plenum pressure, and hence the actuator jet velocity, has a direct and large effect on the lift, whereas varying the actuation frequency has only a small effect. At the maximum pressure allowed by the wing, the mass flow rate is measured to be 9.26×10^{-4} kg/s at 34.5 kPa. The leading edge is tapered with a 5:1 elliptic shape, and the thickness-to-chord ratio is 0.069. The centerline chord-based Reynolds numbers ranged from $Re_c = 62,000$ to 140,000. The microvalves, pressure regulator, shutters, and data acquisition are controlled with Simulink® models, dSPACE® software, and a ds1104 analog-to-digital/digital-to-analog converter interface running at a sample rate of 10 kHz. Force balance, velocity information, and pressure data are acquired at a sampling rate of 1 kHz.

The time response of the actuator jet velocity is limited by the bandwidth of the pressure regulator, the volume of the plenum, and associated plumbing. Jet velocities, measured with a hot-wire anemometer located in the center of an actuator jet, exhibit a first-order dynamic response with a time delay. Time delays between the desired pressure input signal and the jet exit velocity, due to the time required to pressurize the plenum volume within the wing, range from 0.015 s ($t^+ = 0.5$) to 0.030 s ($t^+ = 1$). A nominal model from a family of identified models, from desired pressure to jet velocity, has a time delay of 0.023 s ($t^+ = 0.8$). A comparison of experimental jet velocity and a model of the jet velocity are shown in Fig. 2, plotted as the jet velocity response to a step input in desired pressure normalized by the maximum jet velocity against the convective time at 7 m/s.

III. Results

A. Plant Identification

The range of possible control is first determined by creating a static map, which is the steady-state lift response to varying the pressure supplied to the actuators. The angle of attack is fixed at $\alpha = 20°$, the microvalves are pulsed continuously at 29 Hz, and the plenum pressure is varied from 1 to 31 kPa in 1 kPa increments. Data are acquired for 60 s at each pressure magnitude, and the mean value of the lift is computed. Figure 3a shows the mean lift response to actuation at flow speeds of 4 through 9 m/s, with the measurements at 5 and 7 m/s repeated as a repeatability test. The data collapse to a single curve when plotted as the change in lift coefficient against the square root of the jet pressure coefficient, and this is shown in Fig. 3b.

To identify dynamic models of the lift response to actuation, modern system identification methods are employed. These techniques require measuring and correlating the system's lift response to pseudorandom binary signal (PRBS) steps in the plenum pressure while operating the actuators at 29 Hz. The change in lift force is defined here as the increment from the steady-state lift that corresponds to actuation at the lower pressure level. One example of the input and output measurements is shown in Fig. 4.

The experiments are repeated at varying magnitudes of input pressures at two flow speeds of approximately 5 and 7 m/s. A family of 21 linear dynamic models was identified using the prediction-error method [12]. First-order models with a time delay of the form

$$G_P(s) = \frac{K}{Ts + 1} e^{-\theta s} \tag{1}$$

represent the data in the mean well (neglecting the high-frequency oscillations), as can be seen in Fig. 4, which compares the measured and simulated responses for one of the identified models. The addition of a time delay in the model results in a significantly better fit of the experimental data when compared with models identified in earlier investigations by the authors [4].

The frequency response of all identified models is shown in Fig. 5. Each model family identified for a fixed flow speed is characterized

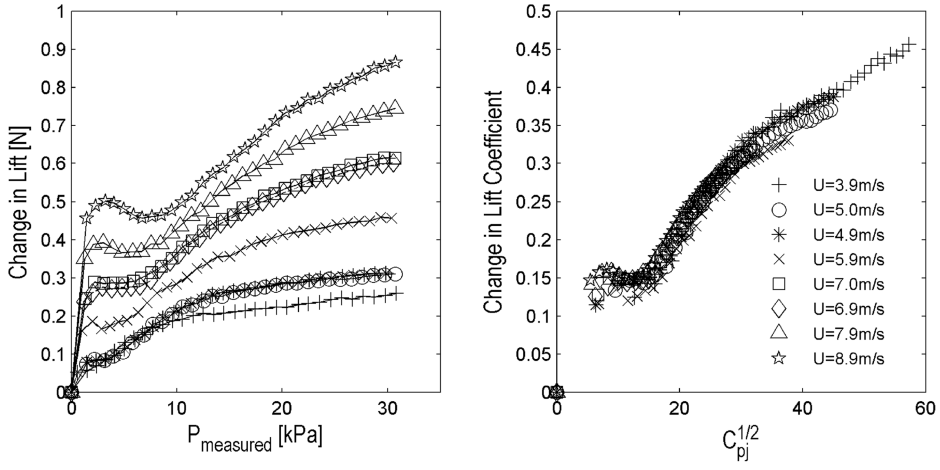

a) b)

Fig. 3 Static maps of lift response to pulsed-blowing actuation at 29 Hz plotted a) against plenum pressure and b) as the change in lift coefficient versus the square root of the jet pressure coefficient.

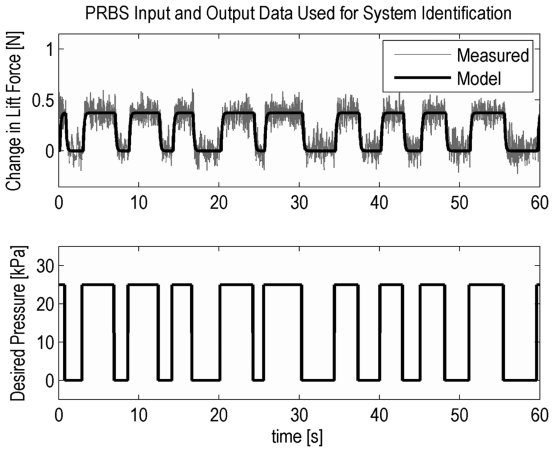

Fig. 4 Example of input–output data used to obtain black-box models of response to pulsed-blowing actuation at 29 Hz.

by a variation of the parameters in Eq. (1): K, T, and θ. This parameter variation between models identified at different actuation magnitudes is due to the nonlinearity seen in the static maps for the different flow speeds shown in Fig. 3a.

The majority of the models identified at the lower flow speed of $U = 5$ m/s show smaller gain than the models identified at $U = 7$ m/s, which is due to the fact that the plant models are defined using dimensional variables. The use of dimensional variables allows for an easier controller design and implementation, since the control objective is to reject disturbances while maintaining a constant lift force.

The control design presented in this paper focuses on achieving good disturbance suppression around a nominal mean flow speed of 7 m/s. Therefore, a nominal model, for use in synthesizing a controller, is found by taking the mean of the transfer functions identified at this flow speed. To obtain a rational transfer function, the dead-time element corresponding to the mean time delay of $\theta = 0.157$ s is approximated by a third-order all-pass transfer function. Its coefficients are determined based on the least-squares method proposed by Frank [20], which minimizes the difference between the step responses of the original and the approximated transfer functions. The phase becomes inaccurate at frequencies larger than about 6 Hz, as can be seen from Fig. 5, but it was not a concern here, because the highest frequency of interest was 3 Hz.

B. Unsteady Aerodynamic Model Identification

The wing response to a longitudinal velocity perturbation is itself dynamic. As discussed in the Introduction, the flow's three-dimensionality and separation render available theory inadequate, so a separate model is identified from the experimental frequency response data. The wind-tunnel speed is oscillated at frequencies

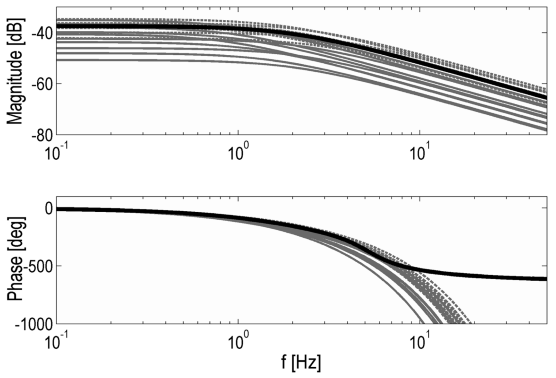

Fig. 5 Frequency response diagram of identified models at flow speeds 5 m/ssolid gray lines) and 7 m/s (dashed gray lines). The solid black line is the nominal model found from the mean of family model parameters for 7 m/s.

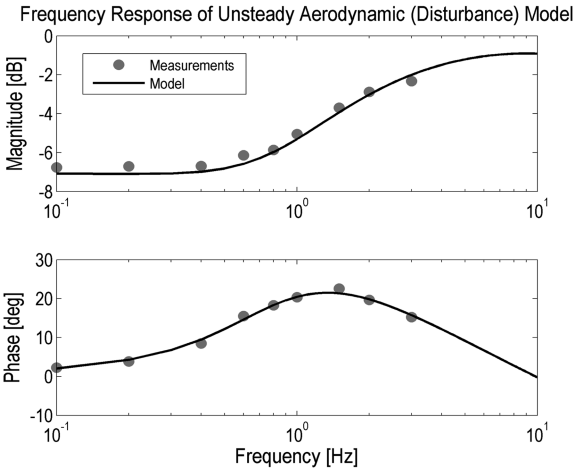

Fig. 6 Frequency response of lift force to longitudinal gusting flow with mean flow speed of 7 m/s.

ranging from 0.1 to 3 Hz, and the lift response of the wing is measured. The cross spectrum between the velocity signal and the lift force is used to obtain the gain and phase of the lift force relative to the velocity at the fundamental frequency. Figure 6 shows the ratio of the lift force amplitude to the velocity amplitude at a mean flow speed of 7 m/s, and the phase between these signals, plotted against the frequency of velocity fluctuations. The frequency response measurements are then used to identify a fourth-order dynamic model $G_d(s)$, shown in Fig. 6 as the solid line. The resulting model becomes the disturbance model in the control architecture, as described in the next section.

C. Controller Architecture

The control objective is to maintain a constant lift force by suppressing lift disturbances caused by flow speed variations, and it is achieved by employing a two-degree-of-freedom controller, shown in Fig. 7. The output y_P of the plant model $G_p(s)$ is perturbed by a disturbance y_d. The actual lift force, $y = y_P + y_d$, is measured and compared against the reference lift value r. A robust feedback controller $K(s)$ regulates the lift force by adjusting the actuation pressure p_j. The closed-loop part of the control architecture provides setpoint tracking at zero steady-state error. This feature accounts for model uncertainties and compensates the disturbances acting on the plant at low frequencies. The synthesis of the controller is discussed in detail in Sec. III.D.

The output disturbance y_d corresponding to a deviation of the lift force is caused by fluctuations in the flow speed, $d = U'$, and is represented by the unsteady aerodynamic response of the wing model $G_d(s)$. The flow speed is measured in real time with a hot-wire anemometer, which is the input d to the disturbance model. The disturbance information can be exploited by using a feedforward controller $K_d(s)$, which acts on the plant input $u = p_j$ to enhance the disturbance rejection.

To account for actuator saturation due to the limited actuation pressure allowed by the wing, the control loop is augmented with a dynamic antiwindup compensator based on a method suggested by

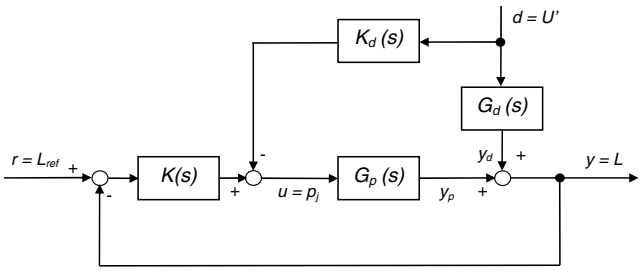

Fig. 7 Controller architecture used for closed-loop experiments.

Park and Choi [21]. It is not shown in Fig. 7 for the sake of conciseness.

D. Controller Synthesis

A robust H_∞ feedback controller is synthesized using the mixed-sensitivity loop-shaping approach [22]. This closed-loop control strategy has been successfully applied in several active flow-control experiments [4,23,24] and is augmented here by a feedforward controller $K_d(s)$ for improved disturbance rejection. By choosing appropriate loop-shaping weights, the control synthesis guarantees robust stability and performance of the closed loop for a given model family. To select the appropriate weights, the maximum deviation of all models $G_p(s)$ (within the model family Π_I) from the nominal model $G_n(s)$ is described by a multiplicative uncertainty $l_I(\omega)$,

$$l_I(\omega) = \max_{G_P \in \Pi_I} \left| \frac{G_p(j\omega) - G(j\omega)}{G(j\omega)} \right| \tag{2}$$

Hence, the model family can be described by

$$\Pi_I\colon\ G_p(s) = G_n(s)[1 + w_I(s)\Delta_I(s)], \qquad |\Delta_I(j\omega)| \le 1, \quad \forall\ \omega \tag{3}$$

where $\Delta_I(s)$ denotes a normalized uncertainty with a frequency dependent weight $w_I(s)$ comprising all identified transfer functions. Figure 8a plots $l_I(\omega)$ and the magnitude of the corresponding weight $|w_I(s)|$ for the family of models identified for the wing. The uncertainty could be reduced by inverting the static map shown in Fig. 3 for one fixed flow speed and using it as a precompensator to account for the steady-state part of the nonlinearities. This was examined in earlier experiments [4], but it turned out not to be necessary in the current control design, because the closed-loop performance is ultimately limited by the time delay of the plant transfer function. This limitation will be discussed further.

To tune the controller, one considers the closed-loop response of the nominal plant, which is given by

$$y = \underbrace{\frac{G_n K}{1 + G_n K}}_{T} r + \underbrace{\frac{1}{1 + G_n K}}_{S} \underbrace{(1 - G_n K_d G_d^{-1})}_{S_d} G_d d \tag{4}$$

where T represents the complementary sensitivity function related to tracking performance and measurement noise, S denotes the sensitivity function related to suppression of disturbances acting on the output of the closed-loop system, and S_d can be interpreted as a feedforward sensitivity function [22]. The sensitivity function and the complementary sensitivity function are shaped by the weights $w_p(s)$ and $w_T(s)$, respectively. A third weight $w_u(s)$ is used to put a bound on the control effort KS, where K is the closed-loop controller and S is the sensitivity defined in Eq. (4). To obtain the controller, a cost functional

$$\min_K \|N[K(s)]\|_\infty, \quad \text{with} \quad N = [\, w_P S \quad w_T T \quad w_u K S\,]^T \tag{5}$$

is minimized, where $K(s)$ denotes the optimal stabilizing controller [22]. The frequency response of the closed-loop transfer functions with the corresponding loop-shaping weights is shown in Fig. 8b. Note that the plant model was normalized using the maximum error and allowable input pressure during the loop-shaping process to allow for easier choice of weights. Adjusting the weight $w_T(s)$ such that

$$|T(j\omega)| < 1/|w_I(j\omega)|, \quad \forall\ \omega \tag{6}$$

ensures robust stability of the closed-loop system for all models identified for the flow speeds 5 and 7 m/s. Note that the magnitude of the uncertainty $|w_I(j\omega)|$ exceeds unity for frequencies larger than approximately 2 Hz. This puts an upper limit on the achievable bandwidth ω_{BT} with respect to the setpoint tracking performance. However, Fig. 8b reveals that the magnitude of the complementary sensitivity T is still well below this limit.

Since the input d to the disturbance model G_d can be measured online, the bandwidth can be improved by using a feedforward controller K_d. If the disturbance and plant model are exact, perfect control could be achieved with $K_d = G_n^{-1} G_d$ [22]. However, the identified plant transfer function contains a positive zero corresponding to the approximation of the time delay and a pole excess of one. The former leads to an unstable inverse of the plant transfer function, and the latter results in a noncausal ideal feedforward controller. These problems can be circumvented by choosing

$$K_d = G_F \tilde{G}_n^{-1} G_d \tag{7}$$

Here, $\tilde{G}_n$ denotes the all-pass-free part of the nominal plant model to yield a stable inverse, and G_F represents a fast first-order filter to render the transfer function K_d causal. Neglect of the time delay, in the feedforward control, and uncertainties in the modeling is compensated for by the closed-loop control. Figure 9 shows that the feedforward controller increases the bandwidth of the controlled plant with respect to the measured disturbances to about 0.7 Hz. However, this comes at the price of increasing the sensitivity even further at a frequency band above approximately 0.8 Hz.

E. Closed-Loop Control Results

The performance of the controller is evaluated by subjecting it to a pseudorandom velocity signal (PRS). The voltage signal to the shutters, at the downstream end of the test section, is constructed of pseudorandom amplitude steps summed with pseudorandom

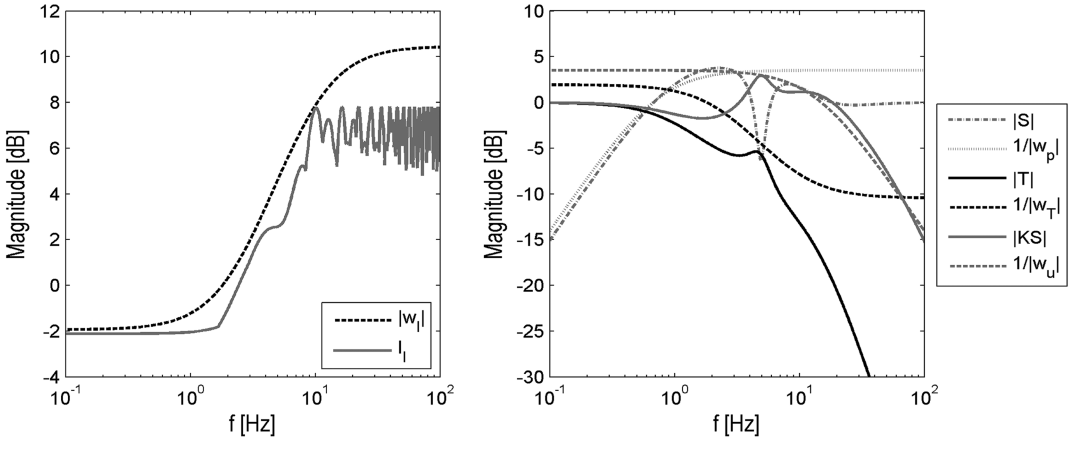

Fig. 8 Multiplicative uncertainty for a) identified model family and b) loop-shaping weights with corresponding transfer functions for synthesized H_∞ controller.

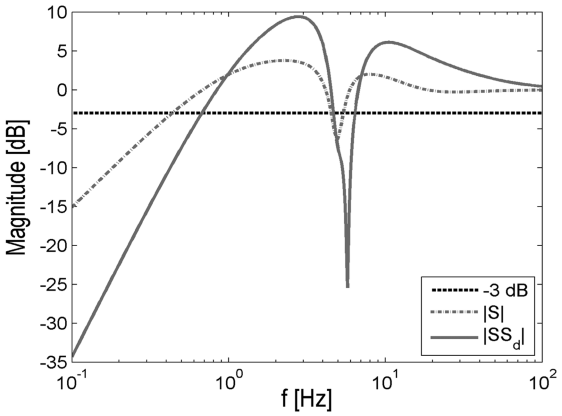

Fig. 9 Frequency response of plant output to sinusoidal disturbances in flow speed for feedback controlled plant (dashed gray line) and feedback controlled plant augmented by feedforward disturbance compensation (solid gray line).

amplitude sinusoidal signals of frequencies less than 1 Hz. Figure 10a shows the magnitude of the velocity plotted against time, and Fig. 10b shows the power spectrum of velocity. The velocity ranges from a minimum of 6.25 m/s to a maximum of 7.25 m/s, with the mean flow speed of 6.9 m/s. The same signal is repeated 15 times to reduce the uncertainty in the amplitude of the power spectrum to below 26%, and the resulting time series measurements are averaged to reduce uncorrelated measurement noise.

The controller is commanded to maintain a constant reference lift of 1.8 N during the PRS experiments. The reference lift is above the maximum value of the uncontrolled lift, and it was selected to reduce the effect of measurement noise. Figure 11 shows the averaged experimental controlled and uncontrolled lift force time series along with simulation results and the desired lift force. The simulation results are obtained using the averaged, experimentally measured velocity profile as an input to the disturbance model and the same reference lift from experiment. The resulting signals are passed through the closed-loop and feedforward disturbance compensators and the plant model response to actuation. Without control, the lift reaches a minimum of 1.1 N and a maximum of 1.5 N. With control, the lift ranges from 1.7 to 1.88 N, where the minimum is from a point where the actuator input is saturated and the required change in lift exceeds the maximum possible value.

Figure 12 shows the power spectrum of the controlled and uncontrolled lifts. Fifteen records of the length of an entire period of the PRS are used in calculating the power spectrum, again giving an uncertainty in the amplitude of the spectrum of less than 26% and a frequency resolution of approximately 0.01 Hz. The controlled case shows an amplification of lift fluctuations, over the uncontrolled case, from approximately 1 to 5.5 Hz.

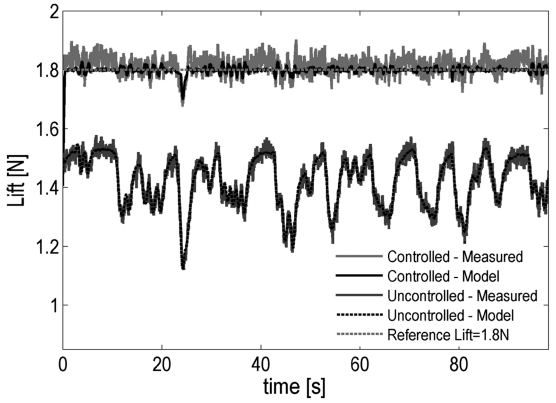

Fig. 11 Phase-averaged controlled and uncontrolled lift time series and comparison with model(s).

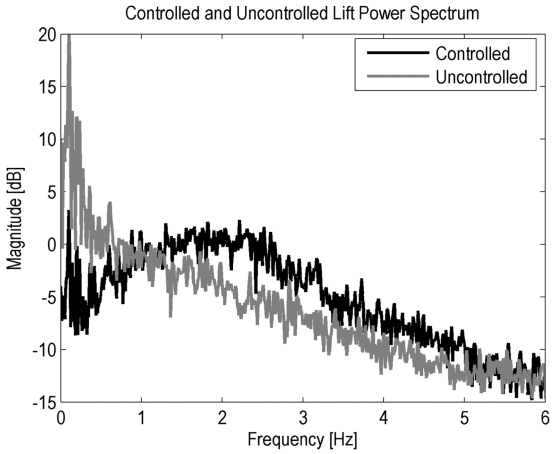

Fig. 12 Power spectrum comparison of fluctuating lift force during controlled and uncontrolled pseudorandom velocity input experiments.

IV. Discussion of Results

The simulation results shown in Fig. 11 agree well with the experimental results, suggesting that the unsteady aerodynamics and dynamics of the response to pressure actuation are captured well by the linear models for the investigated range of operating conditions at a fixed angle of attack, even though the underlying physical process is nonlinear. The agreement also suggests that the linear superposition of the response to actuation y_p and the unsteady aerodynamic response y_d has validity for practical controller synthesis. The use of linear models enables the use of a wide range of relatively simple controller synthesis techniques and analysis tools.

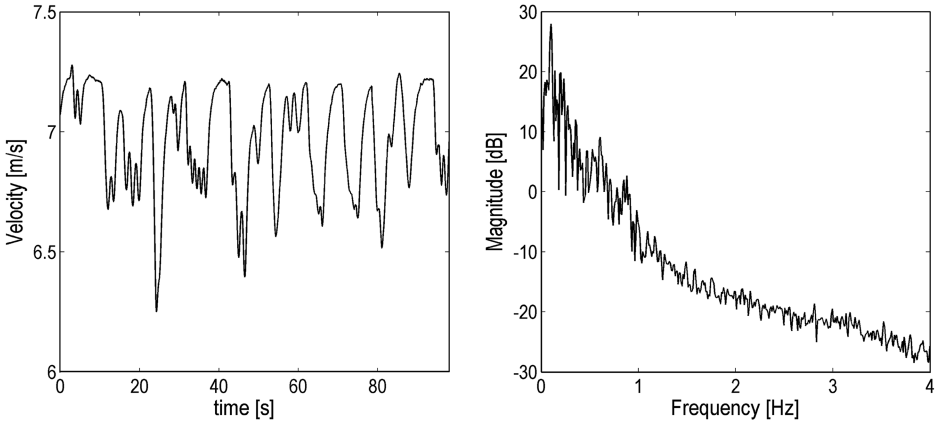

a) Velocity time series **b) Velocity power spectrum**

Fig. 10 Velocity: a) measured pseudorandom time series and b) power spectrum used to test controller.

The nominal time delay from the desired pressure input to the actuator jet velocity response is 0.023 s ($t^+ \approx 0.8$), while the nominal time delay from the desired pressure to lift increase is 0.157 s ($t^+ \approx 5$), which indicates the time delay from jet velocity to the initiation of lift increase of $t^+ \approx 4$. The wing will travel four chord lengths before the disturbance created by the actuators leads to the modified flowfield that leads to an enhanced lift force. It is this fluid dynamic time delay that limits the bandwidth of possible control for the chosen control architecture. We note that this method of actuation does not show the initial reversal in normal force, circulation, or lift, as seen in [4,5,9], which is believed to be due to the relatively slow first-order behavior of the external pressure regulator used to control the actuator jet velocity.

Limitations on the bandwidth of control arise, on the one hand, from constraints on the physically possible control effort and, on the other hand, from the right-half-plane (RHP) zeros corresponding to the approximation of the time delay θ in the nominal model. It can be shown that, for systems with time delays, the closed-loop bandwidth is limited to be less than $1/\theta$ [22]. Because of these limitations, a bandwidth of about $\omega_B \approx 2.7$ rad/s or 0.43 Hz is achieved when just considering the feedback part of the controller, as can be seen from Fig. 9. Here, the bandwidth ω_B is defined as the frequency where the sensitivity S crosses the -3 dB line for the first time from below. Note that the feedback controller shows poorer performance than the uncontrolled case in a frequency band above approximately 0.7 Hz. This can be explained by the so-called second waterbed formula, which is based on a weighted sensitivity integral [22]. It states that reducing the sensitivity of a plant with RHP zeros at low frequencies will cause a large peak in the sensitivity over a limited frequency range. The controller is capable of suppressing disturbances when the overall sensitivity is below one, and disturbances are amplified when the overall sensitivity is greater than one. The controller is effective at reducing lift fluctuations at low frequencies, less than approximately 1 Hz ($k = 0.09$), but it begins to amplify disturbances above this frequency, as can be seen in Fig. 12. This region of amplification agrees reasonably well with the region where the closed-loop sensitivity is greater than 0 dB, as seen in Fig. 9, again suggesting that the linear models capture the dynamics well.

The relatively low bandwidth of the pressure regulator and the time delay between step inputs of desired pressure to jet velocity raises the question: If a faster actuator is used, would the bandwidth of control be increased? A zero-net-mass-flux (ZNMF) wing of a similar planform to the pulsed-blowing wing with piezoelectric actuators [25] shows negligible time delay between a desired input signal and measured output jet velocity. Consequently, the bandwidth of the piezoelectric actuators is an order of magnitude larger than the bandwidth of the pulsed-blowing actuators. The ZNMF wing does show the initial reversal in lift (nonminimum phase behavior), as observed by [5–8]. The nonminimum phase behavior implies at least one RHP zero in the transfer function. A pure RHP zero imposes control limitations at either low or high frequencies [22]. One can achieve tight control at frequencies below approximately $z/2$, where z is the magnitude of the RHP zero, or at frequencies above $2z$, by reversing the sign of the controller gain. Black-box models derived from PRBS voltage inputs to the piezoelectric actuators, which agree well with measured data, show a peak undershoot at $t^+ \approx 1.2$ and have a RHP zero located at 16.5. This zero implies the ability to achieve control below $f \approx 1.3$ Hz ($k = 0.12$) or control above $f \approx 5.3$ Hz ($k = 0.48$), which is comparable to the region where disturbances are amplified with the pulsed-blowing wing modeled with a pure time delay. As a result, even with faster actuators, the range of frequencies of possible control is limited by the flowfield's response to actuation, and not the bandwidth of the actuators.

The first-order models with time delay fit the measured data much better than the previous modeling with first-order models [4]. The improved modeling leads to a better agreement between experiment and theory. The range of frequencies of the current controller is increased over the range in [4]. This is, on the one hand, due to the incorporation of an unsteady aerodynamic model and the feedforward disturbance compensation. On the other hand, the better modeling also improves the performance.

A number of important challenges must be addressed before a practical gust-suppression system can be implemented on a flight vehicle. The dependence of the plant and unsteady aerodynamics models on angle of attack and vertical motion of the flight vehicle has not been addressed. Including these effects will most likely require a nonlinear control system to be designed. Furthermore, gust sensing and measurements of the instantaneous lift for practical flight vehicles are additional issues to be resolved. The determination of the instantaneous load acting on the aircraft may be accomplished by differential surface pressure measurements, accelerometers, velocimetry, or combinations of these measurements.

V. Conclusions

The current effort to suppress lift oscillations in an unsteady freestream with closed-loop control shows reductions in the fluctuating lift at reduced frequencies $k < 0.09$. The range of frequencies where suppression is achieved is nearly double the bandwidth of previous closed-loop control attempts. The improved performance is attributed to better modeling of the plant (with time delay) and the use of a feedforward section in the controller architecture to account for the unsteady aerodynamic effects. The linear models are capable of predicting the lift response to pressure actuation and unsteady aerodynamics within the range of flow speeds and conditions investigated; this can be seen by the comparison between the experimental and simulation results. Additionally, the assumption of linear superposition of the response to pulsed-blowing actuation and the varying freestream velocity is valid for the experimental conditions examined (i.e., longitudinal gusts and fixed angle of attack).

The bandwidth of control is shown to be limited by the separated flow's response to actuation, and not the bandwidth of the actuator. The time delay present in the pulsed-blowing system model is responsible for limiting the bandwidth. This time delay is related to the time for the disturbance created by the actuators to convect over the wing and establish the new flowfield that leads to an increase in lift. Even with faster actuators, the RHP zero, present in a lift response model of the ZNMF wing, limits the control over a similar range of frequencies to the pulsed-blowing wing. These results suggest an upper limit on the frequency response that can be achieved on a wing using the present architecture. Efforts to improve control within these limitations should concentrate on the control architecture, controlled variables, and algorithms. Efforts to increase the bandwidth of control will most likely concentrate on working to directly affect the mechanism of lift enhancement with an improved understanding of the flow physics.

Acknowledgments

The support for this work by the U.S. Air Force Office of Scientific Research (AFOSR) Multidisciplinary University Research Initiative (FA9550-05-0369) with program manager Fariba Fahroo and AFOSR grant (FA9550-09-1-0189) monitored by Doug Smith is gratefully appreciated. David Williams gratefully acknowledges partial support from the Alexander von Humboldt foundation. The authors also acknowledge partial support from the Illinois NASA Space Grant Consortium for Wesley Kerstens and support from the German Science Foundation for Jens Pfeiffer.

References

[1] Hoblit, F. M., *Gust Loads on Aircraft: Concepts and Applications*, AIAA Education Series, AIAA, Washington, D. C., 1988, pp. 1–122.

[2] Seifert, A., Bachar, T., Koss, D., Shepshelovic, M., and Wygnanski, I., "Oscillatory Blowing: A Tool to Delay Boundary Layer Separation," *AIAA Journal*, Vol. 31, No. 11, 1993, pp. 2052–2060. doi:10.2514/3.49121

[3] Seifert, A., Darabi, A., and Wygnanski, I., "Delay of Airfoil Stall by Periodic Excitation," *Journal of Aircraft*, Vol. 33, No. 4, 1996, pp. 691–698. doi:10.2514/3.47003

[4] Williams, D. R., Kerstens, W., Pfeiffer, J., King, R., and Colonius, T., "Unsteady Lift Suppression with a Robust Closed Loop Controller," *Active Flow Control II*, edited by R. King, Vol. 108, Notes on Numerical

Fluid Mechanics and Multidisciplinary Design, Springer–Verlag, Heidelberg, Germany, 2010, pp. 19–30.
[5] Darabi, A., and Wygnanski, I., "Active Management of Naturally Separated Flow Over a Solid Surface. Part 1: The Forced Reattachment Process," *Journal of Fluid Mechanics*, Vol. 510, June 2004, pp. 105–129.
doi:10.1017/S0022112004009231
[6] Darabi, A., and Wygnanski, I., "Active Management of Naturally Separated Flow Over a Solid Surface. Part 2: The Separation Process," *Journal of Fluid Mechanics*, Vol. 510, June 2004, pp. 131–144.
doi:10.1017/S0022112004009243
[7] Amitay, M., and Glezer, A., "Flow Transients Induced on a 2-D Airfoil by Pulse-Modulated Actuation," *Experiments in Fluids*, Vol. 40, No. 2, 2006, pp. 329–331.
doi:10.1007/s00348-005-0069-6
[8] Brzozowski, D., and Glezer, A., "Transient Separation Control Using Pulse Combustion Actuation," AIAA Paper 2006-3024, 2006.
[9] Woo, G. T. K., Crittenden, T. M., and Glezer, A., "Transitory Control of a Pitching Airfoil Using Pulse Combustion Actuation," 4th Flow Control Conference, AIAA Paper 2008-4324, June 2008.
[10] Williams, D. R., Tadmor, G., Colonius, T., Kerstens, W., Quach, V., and Buntain, S., "The Lift Response of a Stalled Wing to Pulsatile Disturbances," *AIAA Journal*, Vol. 47, No. 12, 2009, pp. 3031–3037.
doi:10.2514/1.45407
[11] Hildebrand, F. B., *Methods of Applied Mathematics*, Dover, Mineola, NY, 1992, pp. 222–294.
[12] Ljung, L., *System Identification: Theory for the User*, 2nd ed., Prentice–Hall, Upper Saddle River, NJ, 1999, pp. 1–121, 168–536.
[13] Kerstens, W., Williams, D., Pfeiffer, J., King, R., and Colonius, T., "Closed Loop Control of a Wing's Lift for 'Gust' Suppression," AIAA Paper 2010-4969, 2010.
[14] Greenberg, J., "Airfoil in Sinusoidal Motion in a Pulsating Stream," NACA TN 1326, 1947.
[15] Theodorsen, T., "General Theory of Aerodynamic Instability and the Mechanism of Flutter," NACA TR 496, 1949.
[16] Leishman, J., *Principles of Helicopter Aerodynamics*, 1st ed., Cambridge Aerospace Series, Cambridge, England, U.K., 2000, pp. 302–414.
[17] van der Wall, B., "The Influence of Variable Flow Velocity on Unsteady Airfoil Behavior," DLR, German Aerospace Center, DLR-FB 92-22, Berlin, 1992.
[18] Williams, D. R., Collins, J., Tadmor, G., and Colonius, T., "Control of a Semi-Circular Planform Wing in a 'Gusting' Unsteady Freestream Flow. I: Experimental Issues," AIAA Paper 2008-3976, 2008.
[19] Williams, D. R., Quach, V., Kerstens, W., Buntain, S., Tadmor, G., Rowley, C., and Colonius, T., "Low-Reynolds Number Wing Response to an Oscillating Freestream with and Without Feed Forward Control," AIAA Paper 2009-143, 2009.
[20] Frank, P., "Optimale Allpassapproximation von Totzeitgliedern im Zeitbereich," *Automatisierungstechnik: AT*, Vol. 44, 1996, pp. 42–43.
[21] Park, J. K., and Choi, C.-H., "Dynamic Compensation Method for Multivariable Control Systems with Saturating Actuators," *IEEE Transactions on Automatic Control*, Vol. 40, No. 9, 1995, pp. 1635–1640.
doi:10.1109/9.412636
[22] Skogestad, S., and Postlethwaite, I., *Multivariable Feedback Control: Analysis and Design*, Wiley, Chichester, England, 1996, pp. 1–66, 163–219, 259–288, 341–382.
[23] Henning, L., Pastoor, M., King, R., Noack, B., and Tadmor, G., "Feedback Control Applied to the Bluff Body Wake," edited by R. King, Vol. 95, Notes on Numerical Fluid Mechanics and Multidisciplinary Design, Springer–Verlag, Heidelberg, Germany, 2007, pp. 369–390.
[24] Heinz, N., King, R., and Gölling, B., "Robust Closed-Loop Lift Control on an Industry-Relevant Civil Aircraft Half Model," *Active Flow Control II*, edited by R. King, Vol. 108, Notes on Numerical Fluid Mechanics and Multidisciplinary Design, Springer–Verlag, Heidelberg, Germany, 2010, pp. 125–139.
[25] Quach, V., Kerstens, W., Williams, D., Tadmor, G., and Colonius, T., "Transient Response of a Wing to Arbitrary Actuator Input," *3rd International Conference on Jets, Wakes and Separated Flows*, Sept. 2010.

A. Naguib
Associate Editor